Article:
Huang, S-S. and Burgess, I.W. (2012) Effect of transient strain on strength of concrete and CFT columns in fire – Part 2: Simplified and numerical modelling. Engineering Structures, 44. 389 - 399. ISSN 0141-0296

https://doi.org/10.1016/j.engstruct.2012.05.052

10 May 2012

Effect of Transient Strain on Strength of Concrete and CFT Columns in Fire – Part2: Simplified and Numerical Modelling

Shan-Shan Huang[a,*], Ian W. Burgess[a]

[a] Department of Civil and Structural Engineering, The University of Sheffield, Sir Frederick Mappin Building, Mappin Street, Sheffield, S1 3JD, UK

* Corresponding author. Tel.: +44 114 222 5726; Fax: +44 114 222 5793. E-mail address: s.huang@shef.ac.uk (S.-S. Huang).

Number of words: 5751 (Main text: Intro to Conclusion)
Number of figures: 21
Number of tables: 7

Abstract

This paper presents finite element analysis on columns of concrete and concrete-filled tubular section. This study has been conducted with *Vulcan*, a specialist structural fire engineering FE program, which has been further developed to incorporate the transient strain of concrete. The implementation of transient strain in *Vulcan* has been validated against a Shanley-like simplified model. A further extension of the simplified model has been carried out in order to provide direct comparability with the FE modelling. The effects of transient strain, considering thermal gradients through the column cross-section, have been evaluated with both the simplified and FE models. Finally, parametric studies on concrete-filled tubular columns, considering the effects of slenderness ratio, reinforcement, the steel casing and thermal gradient within the cross-section, have been conducted using *Vulcan*.

Notation

A	area
B	model width
C_r	damping coefficient of the rotational damper (Nmms)
C_v	damping coefficient of the vertical damper (Ns/mm)
E	Young's modulus
ε	strain
ε_{th}	thermal strain
ε_{tr}	transient strain
F_s	reaction force on spring
F_s^f	spring force recorded at the end of the previous load step
F_s^{pf}	spring force recorded one load step before
k	stiffness at linear-elastic stage
k_{tr}	a constant between 1.8 and 2.35
L	model length
P	applied load
σ	stress
σ_{u0}	ultimate compressive stress at ambient-temperature
T	temperature
θ	rotation
$\dot{\theta}$	velocity of θ
θ_0	initial imperfection
u	vertical movement
$\dot{u}$	velocity of u
x	deformation of spring
$\dot{x}$	velocity of x
x_σ	instantaneous stress-related displacement
x_{th}	thermal displacement
x_{tr}	transient displacement

1 Introduction

The material property of transient strain (TS) of concrete has been investigated by various authors [1-7] over the past few decades. A companion paper [8] has addressed the influence of this property on the buckling of slender concrete columns using a simplified (Shanley-like) model under the assumption that the temperature distribution within the model is uniform. Considering TS was found to cause a considerable reduction of the buckling resistance of the model, irrespective of the concrete material models or loading-heating schemes used. In this paper, analysis using the Shanley-like model used previously is followed by FE analysis on concrete-filled tubular (CFT) columns. *Vulcan*, a structural fire engineering FE application, is used for this study. This software has been further developed to take TS into account. Due to the inherent complexity raised by TS, simply applying a concrete material model which includes the effect does not guarantee that the numerical modelling will give an accurate representation of the structural behaviour. Therefore, given the lack of test data concerning slender reinforced concrete or CFT columns in fire, the implementation of TS in *Vulcan* has to be validated against the simplified model, in which the progressive changes in stresses and strains due to the combination of thermal and mechanical effects can easily be monitored. Further modifications of the simplified model are therefore carried out, to achieve direct comparability with the FE modelling of columns. The effects of TS, considering representative thermal gradients across the column cross-section caused by the low thermal conductivity of concrete, are investigated with both the simplified and FE models. Parametric studies on CFT columns of various slendernesses, reinforcement ratios, steel tube thicknesses and thermal gradients within the column cross-section are then performed with *Vulcan*.

2 Incorporating TS into *Vulcan*

The structural fire engineering FEA program *Vulcan* is used in this study. It specialises in three-dimensional modelling of the structural behaviour of composite and steel-framed buildings in fire. In the formulation of *Vulcan*, beams and columns are represented by three-dimensional 3-noded beam elements [9], as illustrated in Fig. 1. Each of the three nodes of the beam element has six degrees of freedom, three translational and three rotational, in both local and global coordinates. The cross-section of the beam element is divided into a matrix of segments, each of which may have different mechanical and thermal properties.

The model of TS due to Anderberg & Thelandersson [1] was expressed as

$$\varepsilon_{tr} = -k_{tr}\frac{\sigma}{\sigma_{u0}}\varepsilon_{th} \qquad 20°\text{C} \le T < 500°\text{C} \tag{1}$$

An incremental form of this equation was used in the original formulation of the *Vulcan* beam element [10]:

$$\Delta\varepsilon_{tr} = -k_{tr}\frac{\sigma}{\sigma_{u0}}\Delta\varepsilon_{th} \qquad 20°\text{C} \le T < 500°\text{C} \tag{2}$$

Then TS at step n is calculated as:

$$\varepsilon_{tr}(n) = \sum_{i=1}^{n}\Delta\varepsilon_{tr}(i) \tag{3}$$

However, this formulation implies that the stress remains unchanged between adjacent load or temperature steps, which is not always the case. In particular, the stress re-distribution across the cross-section due to an increment of load or temperature could be very significant when a thermal gradient, and the consequent variations of the thermal and transient strains, is taken into account, or when deflection due to buckling occurs. Therefore, ignoring the variation of the stresses between adjacent load or temperature steps may lead to an inaccurate prediction of the structural behaviour under such circumstances.

The *Vulcan* software has been amended to more closely represent the original Anderberg and Thelandersson model. In this formulation the current TS is related to the stress at the end of the previous load or temperature step. The example in Fig. 2 shows a simply supported and longitudinally unrestrained strut (300mm long and 15mm wide square prism of Grade C30 concrete), heated under a constant load of 3kN and subject to a representative temperature distribution across its cross-section. This column's predicted lateral deflection is lower, and its fire resistance is higher, when using the incremental form (Equation (2)) than when using the original (Equation (1)) and it seems more rational to use the latter.

Irrecoverability of TS is one of its inherent properties [1, 5, 7]. However this was not included in the original *Vulcan* model. This property is included by preventing the transient strain component from decreasing between adjacent steps in this modelling. Ignoring this property can lead to totally different results, as shown in Fig.

3, which compares the behaviour of the same column under identical loading and heating as in Fig. 2, with and without the strain irrecoverability.

In the original *Vulcan* model, TS was added onto the Eurocode 2 [11] equations for the uniaxial stress-strain relationship of concrete. However, since TS is only a component of the concrete straining model given by Anderberg and Thelandersson, it is more consistent to apply their full model rather than introducing its TS component into a different model. It is actually found that combining the Eurocode constitutive model with the TS component from A&T leads to very different behaviour compared with the complete A&T model, as illustrated in Fig. 4 for the same column example. Hence, the full A&T concrete model, as applied to the Shanley-like model [8], was implemented in *Vulcan*, although the conversion from the stress-strain relationships to force-deformation relationships for the simplified model is no longer needed in this case. The EC2 equations for the stress-strain relationship of concrete, used in the original *Vulcan* model, were replaced by the formulation for the instantaneous stress-related strain ε_σ in the A&T model.

3 Extension & modification of the Shanley-like model

The Shanley-like model concentrates the entire bending stiffness of a column to a single hinge at its mid-length [8], it does not have direct comparability with *Vulcan*, in which material continuity along the length of the column is taken into account. Therefore, a further development of the Shanley-like model was necessary, and this is presented below:

3.1 Re-positioning the springs

In the original model, the springs were located as shown in Fig. 5a. This arrangement is adequate when the emphasis is simply on analysing the effects of TS on the behaviour of the simplified model, but a re-arrangement is needed to enable a comparison between the simplified model and an equivalent rectangular-section column. The springs are moved to the centroids of their corresponding areas of the cross-section, as illustrated in Fig. 5b. This makes it possible to find an optimum number of springs to represent properly the material continuity of the cross-section. To make this change, the original formulations of the model (Equations (2)-(4) in the companion paper [8]) are modified to Equations (4)-(6).

$$\dot{\theta} = \left(P(\theta_0 + \theta)L - \frac{B}{2n}\sum_{j=1}^{n}(j-0.5)\cdot(F_{s,2j} - F_{s,1j}) \right) \Big/ C_r \tag{4}$$

$$\left.\begin{aligned} u &= \frac{x_{1j} + x_{2j}}{2} \\ \theta &= \frac{x_{2j} - x_{1j}}{\frac{(j-0.5)B}{n}} \end{aligned}\right\} \quad \Rightarrow \quad \begin{cases} x_{1j} = u - \dfrac{(j-0.5)B}{2n}\theta \\ x_{2j} = u + \dfrac{(j-0.5)B}{2n}\theta \end{cases} \tag{5}$$

$$\left.\begin{aligned} \dot{u} &= \frac{\dot{x}_{1j} + \dot{x}_{2j}}{2} \\ \dot{\theta} &= \frac{\dot{x}_{2j} - \dot{x}_{1j}}{\frac{(j-0.5)B}{n}} \end{aligned}\right\} \quad \Rightarrow \quad \begin{cases} \dot{x}_{1j} = \dot{u} - \dfrac{(j-0.5)B}{2n}\dot{\theta} \\ \dot{x}_{2j} = \dot{u} + \dfrac{(j-0.5)B}{2n}\dot{\theta} \end{cases} \tag{6}$$

where $F_{s,ij}$ is the reaction force on spring j ($j = 1, n$ from column centre to edge) on either convex side ($i = 1$) or concave side ($i = 2$), x_{ij} is the deformation of the corresponding spring and $\dot{x}_{ij}$ is the velocity of x_{ij}.

3.2 Multiple hinges along column length

The model was extended to include multiple hinges along its length, in order to improve the continuity of displacements in the longitudinal direction of an equivalent column, as illustrated in Fig. 6.

The hinges are all assumed to be identical, since the same temperature distributions, and therefore cross-section properties, at all sections along the length are usually assumed for columns under fire conditions. Most of the characteristics of the single hinge in the original model remain unchanged for this multi-hinge model. Each hinge incorporates a number of springs connecting adjacent struts. The length of each strut, except those at the top and bottom of the model, is L/m, where L is the overall length of the model and m is the total number of hinges. The length of the top and bottom struts is $L/(2m)$. Each hinge has two dampers, one vertical and one rotational. A finite small rotation θ_0 is applied as an initial imperfection to each hinge, to guarantee the uniqueness of numerical solutions; it also pre-defines the direction of deflection.

The boundary conditions at the base of the model represent those at an axis of symmetry, and hence the model is an analogue of an equivalent column of twice the length. Each hinge has two degrees of freedom u and θ. The axial deformations of the springs across a hinge still follow the linear strain-gradient assumption ("plane sections remain plane"), and so Equations (5) and (6) are still valid. Within one single hinge, the springs may have different force-deformation relationships and thermal properties, and may represent various materials at different temperatures.

The A&T constitutive model for concrete at high temperature is again adopted, although some of the formulations for the application of this material model need to be modified according to the geometry of the multi-hinge model. The equation, which is used to convert the stress-strain relationships in the original A&T model to the force-displacement relationships of the springs, should be modified to:

$$\sigma = F_s / A, \quad \varepsilon = \frac{x}{L/m}, \quad E = \frac{L/m}{A} k \tag{7}$$

Therefore, the formulations of the spring displacements and their decompositions are amended accordingly. Equations (8) and (9) are derived from the equations of motion. For Hinge k ($k = 1, m$ from model bottom to top):

$$\dot{u}_k = \left(P - \sum_{i=1}^{2} \sum_{j=1}^{n} F_{s,ijk} \right) \Big/ C_v \tag{8}$$

$$\dot{\theta}_k = \left(P \cdot \left(\sum_{l'=k}^{m-1} \sum_{l=0}^{l'} \theta_l + \frac{1}{2} \sum_{l=0}^{m} \theta_l \right) \cdot \frac{L}{m} - \frac{B}{2n} \sum_{j=1}^{n} (j - 0.5) \cdot \left(F_{s,2jk} - F_{s,1jk} \right) \right) \Big/ C_r \tag{9}$$

The loading scheme for this multi-hinge model is the same as that for the one-hinge model under the transient heating scenario. For an arbitrary hinge, the calculation procedure remains unchanged, although some of the formulations are modified as described previously.

4 Structural behaviour of the multi-hinge model

The behaviour of the multi-hinge model subject to transient heating is shown in this section. An example square-section column (of overall length 300mm) is used, whose specification is given in Table 1.

Convergence tests on the magnitudes of the increments of time Δt, load ΔP and temperature ΔT were performed, which indicated that the values in Table 1 are appropriate. The initial imperfection θ_0 and the damping coefficients C_v and C_r do not affect the buckling load of the model [12], and therefore achieving an optimum in computing time and numerical stability is the main consideration when setting their magnitudes.

Due to the low thermal conductivity of concrete, thermal gradients through a column cross-section are certain to occur when it is subject to rapid heating at its surface, such as by a building fire, although a uniform temperature distribution in the longitudinal direction can be assumed. Therefore, the same symmetric bilinear temperature distribution (Fig. 7) was applied to each hinge to study its effects on the mechanics of buckling of this model. $T_{\min}$ is 50% of $T_{\max}$, subject to a lower limit of 20°C.

Convergence tests on the number $2n$ of springs in each hinge and the number m of hinges along the model length, for this non-uniform heating condition, were conducted. It was found that ten springs per hinge (n = 5) in a five-hinge model (m = 5) are appropriate.

The structural responses of the model, at a load ratio of 0.5, are shown below. The total displacement x and its three components (instantaneous stress-related x_σ, transient x_{tr} and thermal x_{th} displacements) of the pair of springs, at the edges of Hinge 1, throughout the loading and temperature increments, are plotted in Fig. 8.

Unlike the uniform heating case, under the bilinear temperature distribution the individual parts of the spring displacements within a hinge are no longer solely determined by the linear strain-gradient assumption. Although the total displacements x still follow the linear strain-gradient rule, there are significant differences within the distributions of their components x_σ, x_{tr} and x_{th} due to the variation of their thermal conditions. Due to the symmetry of the temperature distribution, the thermal expansions x_{th} are identical for the springs at the 'mirror' locations on each side of a hinge; as the outer springs are hotter than the inner ones, the springs at the edges experience the highest x_{th} and those in the centre have the lowest x_{th} across a hinge. Without TS, in order for the distribution of the

total displacements x across an arbitrary cross-section to remain linear, this variation of x_{th} causes additional compression (due to larger compressive x_σ) on the outside and reduced compression, or even induces tension, in the centre. On the other hand, when including TS, this variation of x_σ due to the thermal gradient is less significant compared to its 'No TS' counterpart. This is because, apart from its effect on x_{th}, the thermal gradient also induces a non-uniform distribution of x_{tr} within a hinge. This reduces the variation between the outer and inner values of x_σ which is necessary to keep the cross-section plane.

Fig. 9 plots the relationships between the force F_s^f and the displacement x_σ^f of the springs at the edges and in the centre of Hinge 1, at the end of each load or temperature step during the period of Fig. 8. The differences in x_σ due to the thermal gradient, described previously, result in corresponding differences in the forces F_s between the outer and inner springs. Similarly, this variation of F_s within a hinge is more significant without TS than when it is included. The 'No TS' section of Fig. 9 shows high compression on the edge springs while the central springs are in tension considerably before buckling occurs. Significant variations of the forces and displacements between the outer springs on each side are only observed at buckling.

Under bilinear temperature distribution, considering TS still results in a considerable reduction of the buckling temperature from the case when it is excluded, but this reduction is not as high as when the temperature distribution is assumed to be uniform, as shown in Fig. 10. Various thermal gradients ($T_{\min}/T_{\max}$ = 0.3, 0.7 and 0.9), apart from that ($T_{\min}/T_{\max}$ = 0.5) described previously, have also been applied. The numbers attached to the curves are the corresponding values of $T_{\min}/T_{\max}$. It should be noted that the applied loads (y-axis) in this figure have been nominalised against the critical buckling load at room temperature. The high-temperature strength reduction factors for normal-weight concrete given by Eurocode 2 [11] have also been plotted for comparison. Without TS, the buckling temperatures at any given loading under these bilinear temperature distributions are lower than those under uniform heating. This results from the significantly higher internal force level in the outer compression zone of each hinge with the thermal gradients than when uniform heating is assumed. Although the inner springs are cooler than in the

comparable uniform heating case the thermal gradient makes them act in tension, and so their contribution to the model's overall flexural stiffness is rather modest, because of the low tensile strength of concrete. As mentioned before, this effect of thermal gradient on the internal spring force levels nearly vanishes when including TS. As a result, the buckling resistances of the model under the two heating conditions are similar. This explains why the reduction of the buckling temperature due to TS is less significant under thermal gradients than when assuming the temperature distribution is uniform.

5 Validating *Vulcan* against the simplified column model

In order to validate the implementation of TS in *Vulcan*, the concrete column which has been simulated with the multi-hinge model in Section 4 was also analysed in *Vulcan*. Unlike the simplified model, the full length of the column was modelled.

A general description of the geometry of the model is shown in Fig. 11. To pre-define the direction of buckling, an initial imperfection was introduced by applying a small point load in the x-direction at mid-span. Each node has six degrees of freedom, three translational (Dx, Dy and Dz) and three rotational (Rx, Ry and Rz). In order to model the buckling of the simply supported and longitudinally unrestrained column, the following boundary conditions were assumed:

- N1 (the bottom node) has restraint to Dx, Dy and Dz;
- Dx and Dy of the top node are fixed;
- All the nodes are restrained from rotating about the z-axis (Rz) to avoid twisting;
- All other nodal DoFs are free.

Fig. 12 illustrates an arbitrary cross-section of the model and the distribution of temperature among the segments. In order for this temperature distribution to be the same as in the 2D Shanley-like model, the same bilinear distribution was applied in the direction of buckling (along the x-axis). However, since the simplified model can not cope with the thermal gradients out of the buckling plane, a uniform temperature distribution was adopted in the y-direction. As in the simplified model, any temperature variation along the column length was ignored. Convergence tests on the sensitivity of results to the number of elements along the model length and

the number of segments in each cross-section were performed, for cases both with and without TS under either uniform or non-uniform heating. It was found that four elements along the model length and 100 cross-sectional segments (10 rows by 10 columns) per element were adequate.

Fig. 13 compares the predicted buckling temperatures of the concrete column under different loadings, from both *Vulcan* and the simplified model. Irrespective of the temperature distribution across the column cross-section, or whether TS is considered, the results of the two approaches agree with each other. This indicates a successful validation of *Vulcan's* method of implementing TS against the simplified model, for which the progressive changes in stresses and strains due to the combined thermal-mechanical effects have been well studied. Therefore, the beam elements of *Vulcan*, which take into account the transient straining of concrete, proved to be suitable for further use in the parametric studies on concrete-filled steel hollow-section columns.

6 Modelling of fire tests on concrete-filled columns using *Vulcan*

This section presents a comparison of *Vulcan* analyses with experiments on CFT columns under fire conditions. Given the lack of test data for columns in the range of slenderness interested in this research, three CFT columns [13], which were of intermediate slenderness and failed by overall buckling, were modelled. The columns were all compressed without eccentricity and with both ends fixed against rotation. They were 3760mm long (excluding the end plates) and the middle 3048mm of the length was subjected to the ASTM-EI19 [14] standard fire. The specifications of the columns and their failure temperatures are shown in Table 2.

These tests were modelled in *Vulcan* in the way described in the previous section, except that all DoFs of the top and bottom nodes (except Dz of the top node) were restrained in order to simulate the fixed supports at both ends of the column, with the loaded end free to elongate axially. Sensitivity analyses on the number of elements along the model length and the number of segments in each element showed that six elements along the model length and a 12*12 grid of segments per element were adequate. Given the type of element adopted, slip between the segments of a beam element can not be simulated, which means that the steel casing remains fully in contact with the concrete core in the model.

The temperature distribution along the length of the heated part of the column is considered to be uniform, while the unheated parts remain at 20°C. The published temperature data for these tests is not adequate to establish appropriate temperature distributions across the column cross-section, and these were therefore determined from *Vulcan* thermal analyses. The furnace temperature was in accordance with the ASTM-EI19 [14] standard temperature-time curve, given by:

$$T_f = 20 + 750\left(1 - \exp\left(-3.79533\sqrt{t}\right)\right) + 170.41\sqrt{t} \tag{10}$$

where t is the fire exposure time in hours and T_f is the furnace temperature in °C.

The thermal properties of the tested columns are not given in the literature, and so the Eurocode 4 [15] models for normal-weight concrete and structural steel in fire are applied. The other data assumed in the thermal analysis are *Vulcan* default values, shown in Table 3. In this table V_1, V_2, V_3 and V_4 are the radiation view factors for the fire-exposed surfaces which are horizontal, vertical, between 0°-45° and between 45°-90° to the horizontal, respectively. Since the fire-exposed surfaces of the columns are all vertical, V_2 is applied to all four faces.

The predicted times to buckling given by *Vulcan* are compared with the test results in Fig. 14. The comparison is reasonably good. The difference between the experimental and numerical results occurs mainly because the temperature distributions within the specimens can not be predicted exactly by thermal analysis, due to the lack of information about their thermal properties.

7 Parametric studies on concrete-filled steel columns using *Vulcan*

This section presents parametric studies on CFT columns, which investigate the effects of TS on columns of different slenderness, tube thickness, reinforcement ratio and thermal gradient. The analysis was carried out using *Vulcan* and the models were established in the same way as for the concrete column in Section 5.

The type of element adopted does not allow the simulation of the slip between the steel casing and concrete core. This means that the two materials will remain fully in contact in the model (hereafter referred to as the 'full-contact' scenario). Ding and Wang [16] indicated that whether slip or an air gap is assumed between the steel casing and the concrete infill in the numerical modelling has insignificant influence on the calculated column fire resistance time. This partially justifies the previously

mentioned simplification. However, due to the very high degree of complexity of the interactions between the two materials and the much higher temperature of the steel tube than that of the concrete infill, it is common practice in structural fire design to exclude the steel tube and conduct the design solely utilising the concrete core, in order to achieve conservative results. This scenario is also simulated in this analysis by assuming full loss of the strength of the steel tube at elevated temperatures (referred to as the 'no-tube' scenario hereafter). In this way, although the contribution of the steel casing to the capacity of the column vanishes, its contribution to the temperature distribution across the column cross-section remains.

The temperature distribution along the length of the column is considered uniform, while its distribution across the cross-section is given by the *Vulcan* thermal analysis. In the thermal analysis, each column is assumed to be heated on all four faces. The temperature of the fire rises according to the ISO-834 [17] standard temperature-time curve which is given by:

$$T_g = 20 + 345 \log_{10}(8t + 1) \tag{11}$$

where t is the fire exposure time in minutes and T_g is the gas temperature in °C.

The thermal properties for normal weight concrete, structural steel and steel reinforcement in fire given in Eurocode 4 [15] are applied. The other data assumed in the thermal analysis are *Vulcan* default values, as previously shown in Section 6.

7.1 Thickness of steel tube

This section investigates whether the steel casing thickness of CFT columns has any influence on the stability of such columns when TS is included. Three slender CFT columns, of identical width and length but different steel casing thicknesses, were analysed. The columns were all 3m long, 150mm wide and of square cross-section, which means that the slenderness ratios of the columns were each equal to 69. Grade S355 steel and C30 concrete were adopted for the steel hollow section casing and concrete infill, respectively. The tube thicknesses of the columns are shown in Table 4. At ambient temperature, buckling failures were observed for all three columns. Their buckling loads are also shown in Table 4, compared to their compressive (crushing) strengths, without considering the strength enhancement of the concrete core due to the confinement from the steel tube.

Fig. 15 shows the gas temperature and the temperature distributions across a quarter of the cross-section of the three columns. Significant thermal gradients between the inner core and the periphery are seen in all three columns. The difference in temperature between the steel tubes of the three columns is evident; the thinner the tube, the higher the temperature at Point 1. Due to the low conductivity of concrete, the temperature distributions in the concrete cores of the three columns are similar. At some points the previously-mentioned relationship between the temperature and tube thickness reverses as the fire temperature rises. For instance, the temperature at Point 6, which is right in the middle of the concrete core, is lower for the column with the thinner casing. This results from the increase of the dimension of the concrete core as the tube thickness decreases, given that the overall dimensions of the columns are the same.

Under both the 'full-contact' and 'no-tube' scenarios, reductions of the predicted buckling temperatures when considering TS, compared to the corresponding 'No TS' cases, can be observed in all three columns under any given load, as shown in Fig. 16. It should be noted that hereafter the buckling temperature refers to the temperature at the hottest position, which is shown as Point 1 in Fig. 15, when failure occurs. This reduction of the buckling resistance due to the effect of TS decreases with increasing thickness of the steel casing under the 'full-contact' assumption, whereas this trend reverses in the 'no-tube' scenario. For the former, this phenomenon indicates logically that, as the thickness-to-width ratio of a CFT column increases, the behaviour of the column is more influenced by the behaviour of the steel tube, and therefore the effect of the transient strain of the concrete infill may not be as significant as for concrete columns. On the other hand, under the 'no-tube' assumption, the width of the concrete core decreases when the tube thickness is increased, since the overall dimensions of the columns are identical. This causes an increase of the slenderness of the concrete core and a slight decrease of the thermal gradient between the outer and inner parts of the cross-section. It seems that, when excluding the steel tube, the reduction of buckling temperature due to TS increases with increasing slenderness of the concrete core. However, since the temperature distributions across the cross-sections of the three columns are slightly different, a further study is needed before drawing this conclusion. In addition, in both cases, considering TS results in higher vertical contractions and lateral deflections, and these are more significant in the 'no-tube' scenario.

7.2 Slenderness

In this section, the behaviour of three CFT columns of different slenderness is compared. It should be noted that CF2 is used as a reference column in these parametric studies, in each of which only one parameter varies between the analysed columns. Therefore, the columns evaluated in this section are of the same configurations as those of CF2, apart from their lengths. The length, slenderness ratio and ambient-temperature buckling load of each column are shown in Table 5.

Fig. 17 illustrates the differences in the predicted buckling temperatures between the cases with and without TS for the three columns under various loads. A reduction of the estimated buckling resistance due to the effect of TS occurs, although it is not very significant, to each column under the 'full-contact' assumption. This reduction is also found to increase as the column slenderness increases, except when subject to very high loads. However, in the 'no-tube' scenario, this reduction is only observed from the two more slender columns, CF2 and CF4, under all the loads, and these reductions are more significant than in the 'full-contact' scenario. However, for the very stocky CF5, considering TS results in increases rather than reductions of the buckling temperatures, except at LR = 0.5. Another column, which is even stockier (slenderness ratio = 30) than CF5, was also analysed. The increase of its fire resistance (buckling temperature), due to the effect of TS, occurs across the range of load levels. This suggests that, when the axial displacement of the column dominates over bending, considering TS in the analysis may benefit the estimated fire resistance, due to its relaxation of the thermal expansion. In general, it may be concluded that, irrespective of whether the contribution of the steel tube to the fire resistance of CFT columns is considered or not, the effects of TS on buckling become increasingly significant as the column slenderness increases. Moreover, all three columns experience more vertical contraction and lateral deflection when TS is included than without it and these are more significant in the 'no-tube' scenario than under the 'full-contact' assumption.

7.3 Reinforcement ratio

In this section, the behaviour of two CFT columns (CF6 and CF7), which have different amounts of reinforcement, are compared with that of CF2. Again, this investigation focuses on how TS affects the stability of these columns when subjected to the standard fire. CF6 and CF7 have the same cross-section and length as CF2, except that each of them has four reinforcing bars along its length.

Grade S460 re-bars and the EC4 [15] material properties for reinforcing steel were adopted. The reinforcement ratio A_s/A and the ambient-temperature buckling load of each column are shown in Table 6, where A is the area of the cross-section and A_s is the sum of the areas of the reinforcing bars.

Thermal analyses were again carried out. The variation of the reinforcement ratio between the three columns has very little influence on their temperature distributions across the cross-section, although the re-bars are evidently heated faster than the surrounding concrete.

All three columns experience reductions of their estimated buckling resistances due to the effect of TS under all the applied loads, in both the 'full-contact' and 'no-tube' scenarios, as shown in Fig.18. These reductions are low and almost unaffected by the variation of the reinforcement ratios between the columns under the 'full-contact' assumption. This suggests that in this case the steel casing dominates the behaviour, whereas the contributions of the concrete core and the re-bars are low. In the 'no-tube' scenario, the reductions of the buckling temperature due to TS are more significant than in the 'full-contact' scenario, and decrease with increase of reinforcement ratio. This is simply because the contributions of the concrete core to the behaviour of the columns are more significant when the steel tube being neglected and when the re-bar ratio being lower. Considering TS also results in increases of vertical contraction and lateral deflection in both the 'no-tube' and 'full-contact' scenarios, and these effects of TS are more significant in the former than the latter. In both cases, these effects of TS decrease between the three columns as the reinforcement ratio increases.

7.4 Thermal gradients across the column cross-section

This section presents a study of the impact of the temperature distribution across the cross-section of a CFT column on the extent to which TS affects its buckling in fire. CF2 was re-evaluated under heating at different rates, which introduced different temperature gradients across the column cross-section. Two fires, one faster and one slower in growth than the ISO [17] standard fire, were applied as well as the standard fire itself. Their expressions are given in Table 7.

The results of the thermal analysis of CF2 under the three heating scenarios are shown in Figures 19 and 20. The development of the gas temperature and the temperatures at Points 1, 4 and 6 over the heating time are shown in Fig. 19. The

temperatures at these locations, when the surface temperatures are equal to 615°C in all the three cases, are shown in Fig. 20.

The difference of predicted buckling temperatures between the analyses with and without TS is plotted in Fig. 21 against the applied load level for the three heating cases. Irrespective of the different heating, the TS-induced decrease of the estimated buckling resistance occurs at any given load level; this is again more significant under the 'no-tube' assumption than in the 'full-contact' scenario. Fig. 21 also shows a trend for the effects of TS to decrease with increase of the thermal gradient between the outer and inner parts of the cross-section. A similar effect has already been indicated by the simplified model in Section 4. The underlying mechanics has been explained by examining the internal forces and displacements in the multi-spring model.

8 Conclusions

A fairly common view of the effect of transient strain on concrete parts of structures in fire is that it is generally beneficial, preventing the occurrence of very high localised compressive stresses near to the exposed surfaces of members. This is probably true for elements which are by nature fairly stocky, ensuring that the whole cross-section plays a part in resisting loads as temperatures rise. However this study shows it to be untrue for slender cross-sections under compression. The analyses, using both the simplified model and FE analysis with *Vulcan,* have clearly compared very closely; there is very little difference in the predicted failure temperatures given by the two models under the same loading. Both models indicate that considering transient strain causes a considerable reduction of buckling capacity compared with that predicted without transient strain, but that this reduction is less severe if a thermal gradient, rather than a uniform temperature distribution through the column cross-section, is assumed.

The parametric studies on CFT columns show that including transient strain in the concrete constitutive relationship generally causes an increase of the deflection and a reduction of the buckling resistance. These effects of TS are more significant in the 'no-tube' scenario than under the 'full-contact' assumption, as well as:

- with increasing column slenderness;
- when the thermal gradient between the outer and inner parts of the cross-section is less steep;

- with decreasing tube thickness in the 'full-contact' scenario;
- when the reinforcement percentage decreases in the 'no-tube' scenario, although it has almost no effect when full contact is assumed between the steel tube and the concrete.

In general, the column slenderness and the temperature distribution across its cross-section control the influence of transient strain on buckling at high temperature. Transient strain should not be neglected, especially for columns of slenderness ratios higher than about 70.

It must be recognised that 'full contact' between the encasing tube and the concrete core is not realistic in most heating scenarios. The coefficients of thermal expansion of carbon steels and most types of concrete are within the same order of magnitude, with concrete 'overtaking' steel at around 300°C. However, the speed with which the steel casing heats compared with the concrete core (unless heating is extremely slow) is such that the bond at the core-casing interface will clearly break, and only partial composite action, at best, will occur at the higher fire temperatures. In addition, the expansion of the longitudinal free length of the casing against the much smaller free expansion of the core will cause high compressive stress in the casing, and consequent local buckling, so that the contribution of the casing is greatly reduced.

A final *caveat* is necessary. It has been assumed in these studies that transient strain is a concrete property which can be applied locally and incrementally within a concrete cross-section. Present knowledge suggests that this is the case, but material test evidence in particular is based on experiments in which heating is assumed to have been slow enough to avoid significant thermal gradients during the process of reaching the uniform temperatures at which transient strain is measured. There is still a pressing need to resolve the nature of transient strain at different levels, from the concrete micro-mechanics and chemistry which cause the phenomenon to practical constitutive models to be used in thermo-structural analysis.

Acknowledgment: *The principal author is grateful for the support of Corus Group Ltd and the Engineering and Physical Sciences Research Council of the United Kingdom, under a Dorothy Hodgkin Postgraduate Award.*

References

[1] Anderberg Y, Thelanderson S. Stress and deformation characteristics of concrete at high temperatures. 2. Experimental investigation and material behaviour model. Bulletin 54. Sweden: Lund University; 1976.

[2] Khoury GA, Grainger BN, Sullivan PJE. Transient thermal strain of concrete: literature review, conditions within specimen and behaviour of individual constituents. Mag Concrete Res 1985; 37(132):131-44.

[3] Khoury GA, Grainger BN, Sullivan PJE. Strain of concrete during first heating to 600°C under load. Mag Concrete Res 1985; 37(133):195-215.

[4] Khoury GA. Performance of heated concrete - Mechanical properties. Contract NUC/56/3604A with Nuclear Installations Inspectorate of the Health and Safety Executive. London: Imperial College; 1996.

[5] Khoury GA. Strain of heated concrete during two thermal cycles. Part 1: Strain over two cycles, during first heating and at subsequent constant temperature. Mag Concrete Res 2006; 58(6):367-85.

[6] Schneider U. Properties of materials at high temperatures - Concrete. RILEM 44-PHT. Kassel: University of Kassel; 1985.

[7] Schneider U, Horvath J. Behaviour of ordinary concrete at high temperatures. Research Report Vol. 9. Vienna: Institute of Building Materials, Building Physics and Fire Protection, Vienna University of Technology; 2003.

[8] Huang S-S, Burgess IW. Effect of transient strain on strength of concrete and CFT columns in fire - Part1: Elevated-temperature analysis on a Shanley-like column model. Submitted to Eng Struct xxxx.

[9] Huang Z, Burgess IW, Plank RJ. 3D modelling of beam-columns with general cross-sections in fire. In: Proceedings of the 3rd international workshop on structures in fire. 2004. p. 323-34.

[10] Huang Z, Burgess IW, Plank RJ. Three-dimensional analysis of reinforced concrete beam-column structures in fire. J Struct Eng ASCE 2009; 135(10):1201-12.

[11] European Committee for Standardization (CEN). BS EN 1992: Eurocode 2: Design of concrete structures - Part 1-2: General rules - Structural fire design. Brussels: CEN; 2004.

[12] Huang S-S, Burgess I, Huang Z, Plank R. The mechanics of inelastic buckling using a Shanley-like model. P I Civil Eng-Eng Comp Mech 2011; 164(2):103-19.

[13] Lie TT, Chabot M. Experimental studies on the fire resistance of hollow steel columns filled with plain concrete. IRC Internal Report No. 611. Ottawa: Institute for Research in Construction, National Research Council of Canada; 1992.

[14] American Society for Testing and Materials (ASTM). Standard methods of fire tests of building construction and materials - E119-83. US: ASTM; 1985.

[15] European Committee for Standardization (CEN). BS EN 1994: Eurocode 4: Design of composite steel and concrete structures - Part 1-2: General rules - Structural fire design. Brussels: CEN; 2005.

[16] Ding J, Wang YC. Realistic modelling of thermal and structural behaviour of unprotected concrete filled tubular columns in fire. J Constr Steel Res 2008; 64(10):1086–102.

[17] International Standards Organization (ISO). ISO 834: Fire resistance tests, elements of building construction. Switzerland: ISO; 1980.

Figure Captions

Figure 21 Reduction of the estimated buckling temperature due to the effect of TS, against the imposed load level, for columns under different heating.

Table Captions

Table 1

L (mm)	B (mm)	θ_0 (rad)	C_v (Ns/mm)	C_r (Nmms)	Δt (s)	ΔP (N)	ΔT (°C)
150	15	1E-4	200000	200000	0.001	100	1

Table 1 Specification of the multi-hinge model analysed.

Table 2

Column No.	Width (mm)	Tube Thickness (mm)	Steel Yield Strength (MPa)	Concrete Strength (MPa)	Aggregate	Test Load (kN)	Fire Resistance (min)
SQ-01	152.4	6.35	350	58.3	Siliceous	376	66
SQ-02	152.4	6.35	350	46.5	Carbonate	286	86
SQ-07	177.8	6.35	350	57	Siliceous	549	80

Table 2 Summary of test parameters and results [13].

Table 3

Moisture Content (kg/m^3)	Surface Abortion Factor	Surface Emissivity Factor	Fire Emissivity Factor	V_1	V_2	V_3	V_4
48	0.9	0.9	0.75	1.0	0.5	0.8	0.7

Table 3 *Vulcan* default values used in thermal analysis.

Table 4

	Tube Thickness (mm)	Buckling Load at 20°C (kN)	Crushing Strength at 20°C (kN)
CF1	5	1582	1618
CF2	10	2463	2495
CF3	15	3270	3308

Table 4 Buckling loads and crushing strengths of the CFT columns with various steel tube thicknesses.

Table 5

	Length (m)	Slenderness Ratio	Buckling Load at 20°C (kN)
CF2	3	69	2463
CF4	4	92	2397
CF5	2	46	2463

Table 5 Specifications of the CFT columns of different slenderness.

Table 6

	Re-bar Ratio (%)	Buckling Load at 20°C (kN)
CF2	0	2463
CF6	1.8	2563
CF7	4	2722

Table 6 Buckling loads at 20°C of the CFT columns with various reinforcement ratios.

Table 7

Fast heating	$T_g = 20 + 345\log_{10}(32t + 1)$
ISO fire	$T_g = 20 + 345\log_{10}(8t + 1)$
Slow heating	$T_g = 20 + 345\log_{10}(2t + 1)$

t is the fire exposure time in minutes and T_g is the gas temperature in °C.

Table 7 Gas temperature-time relationships of the three fires.

Figure 1

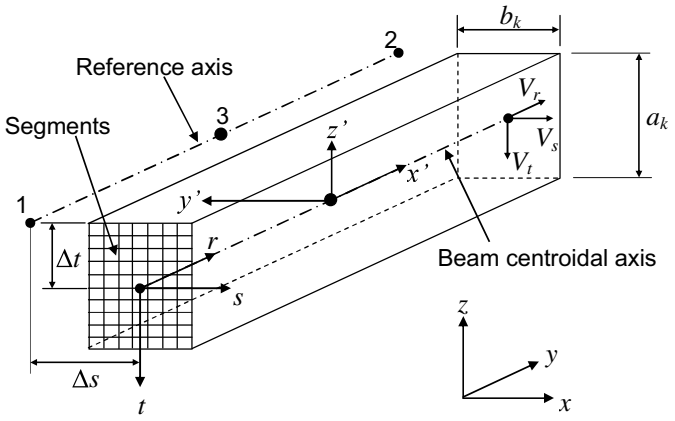

Figure 1 Configuration of the three-dimensional 3-noded beam element [9].

Figure 2

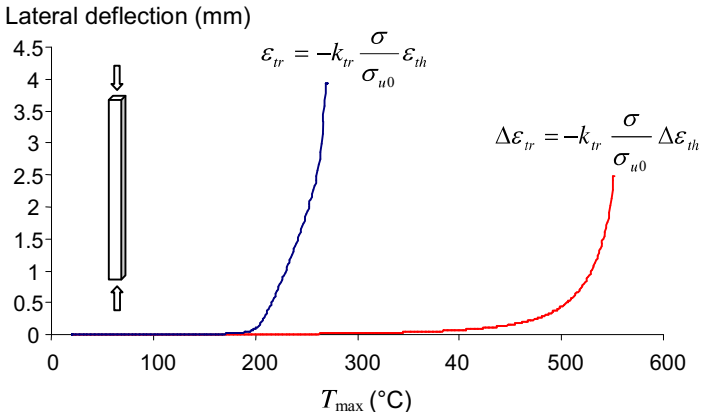

Figure 2 Column deflections using the original and incremental forms of equations for TS.

Figure 3

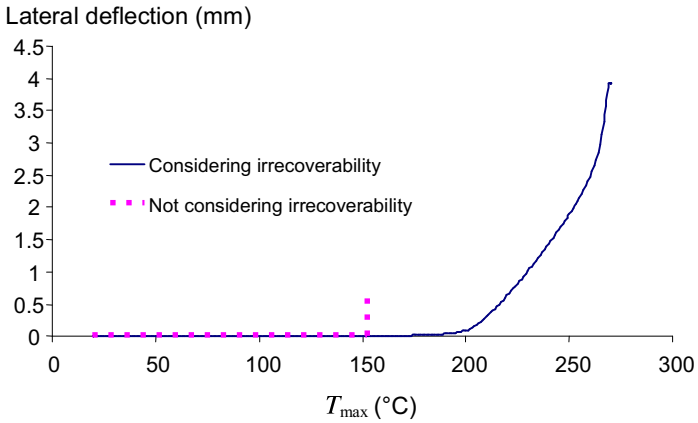

Figure 3 Importance of considering the irrecoverability of TS in numerical modelling.

Figure 4

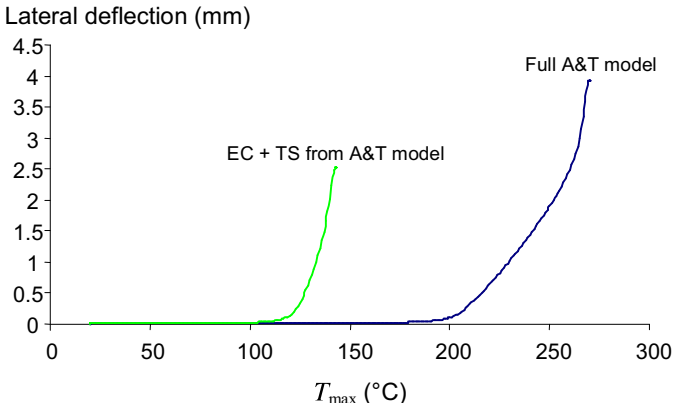

Figure 4 Deflections of the column studied in Figures 2 and 3, from the EC2 concrete constitutive model plus the A&T assumption for TS, and from the full A&T model.

Figure 5

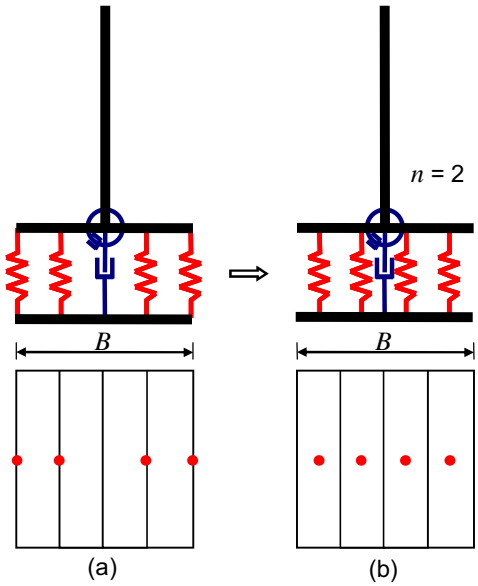

Figure 5 Re-positioning the springs to the centroids of their corresponding areas.

Figure 6

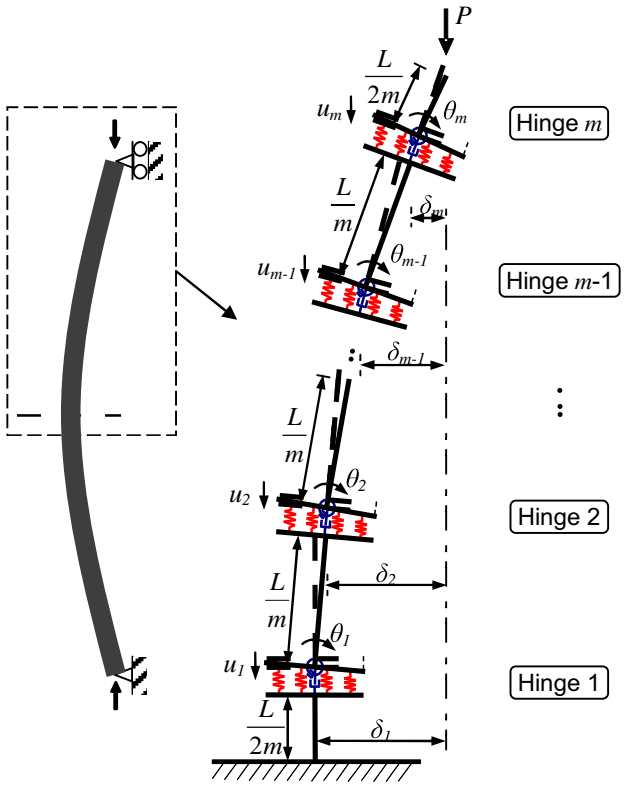

Figure 6 Multi-hinge model.

Figure 7

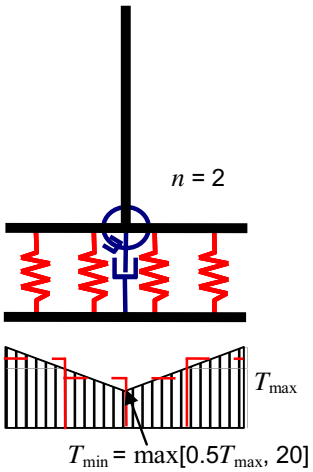

Figure 7 The symmetric bilinear temperature distribution across each hinge.

Figure 8

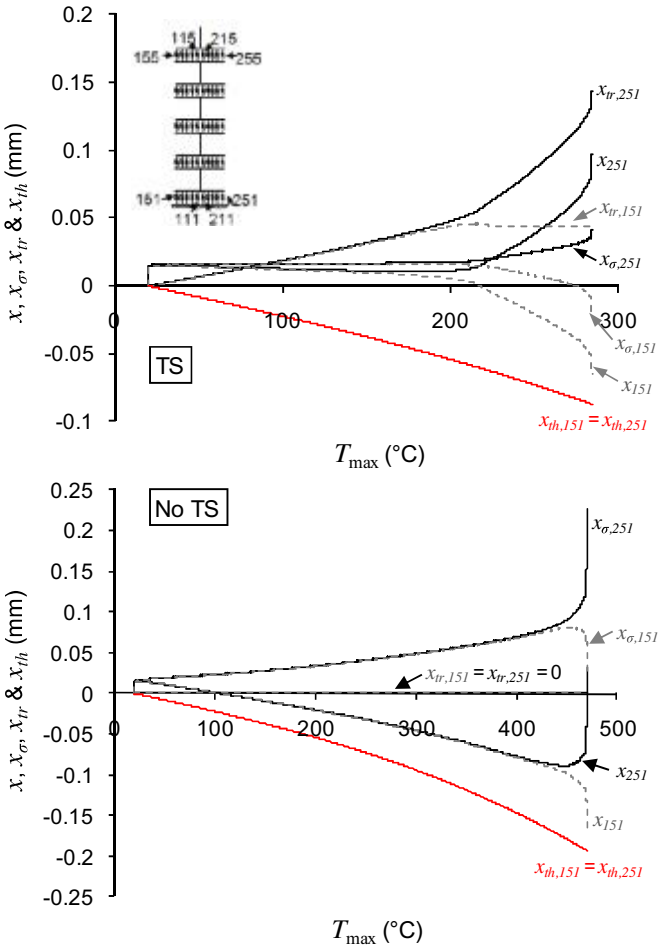

Figure 8 The displacements of the springs at the edges of the bottom hinge, under bilinear temperature distribution.

Figure 9

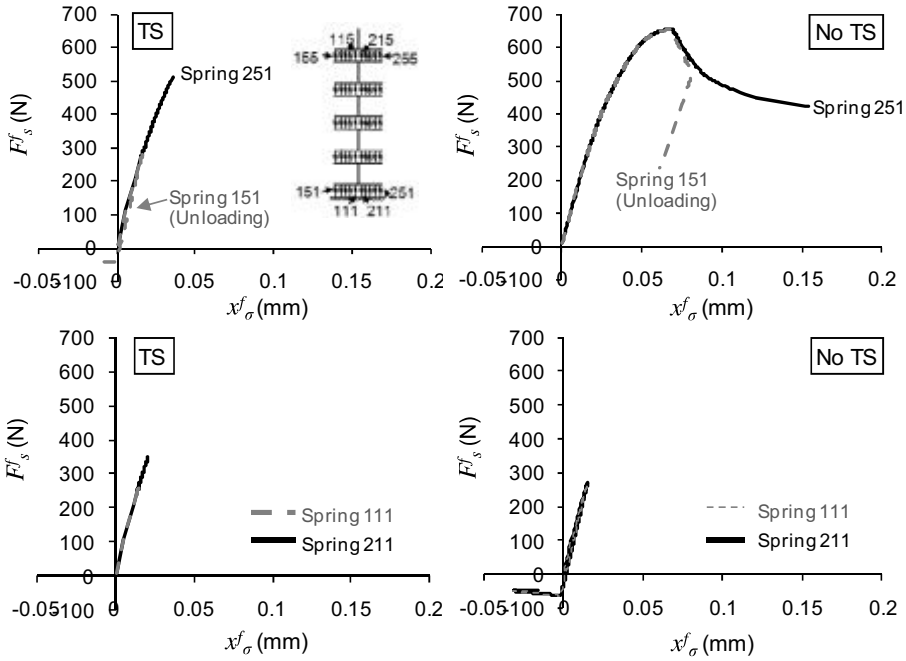

Figure 9 Compressive force-displacement curves of the springs at the edges and in the centre of the bottom hinge, under bilinear temperature distribution.

Figure 10_v2

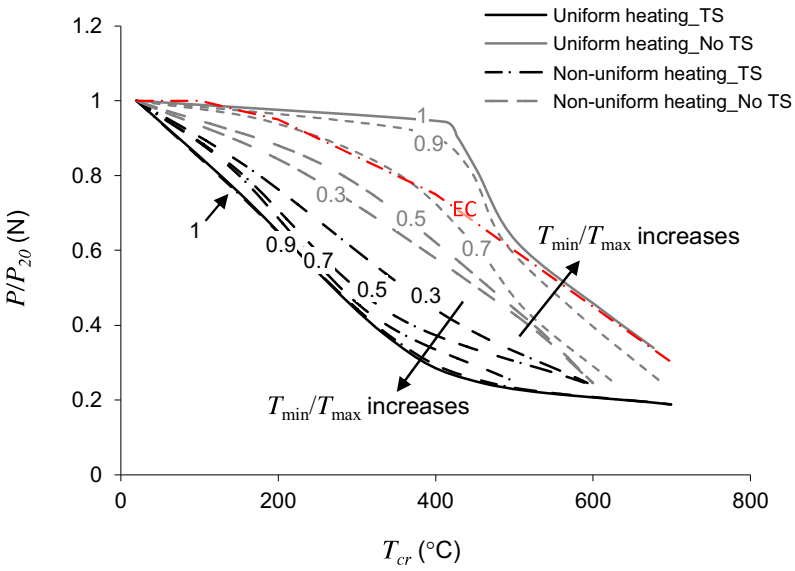

Figure 10 Effect of thermal gradient on the buckling resistance of the model, with and without TS.

Figure 11

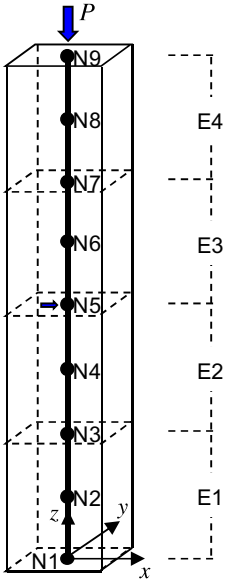

Figure 11 General description of the geometry of the *Vulcan* model.

Figure 12

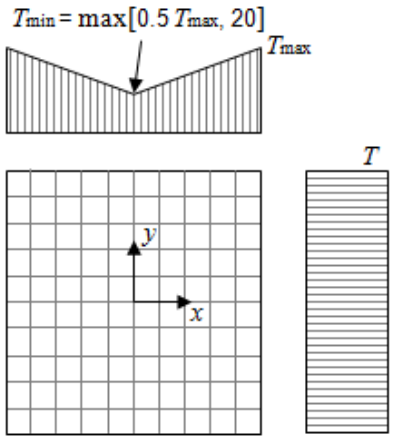

Figure 12 Temperature distribution through a cross-section of the *Vulcan* model.

Figure 13

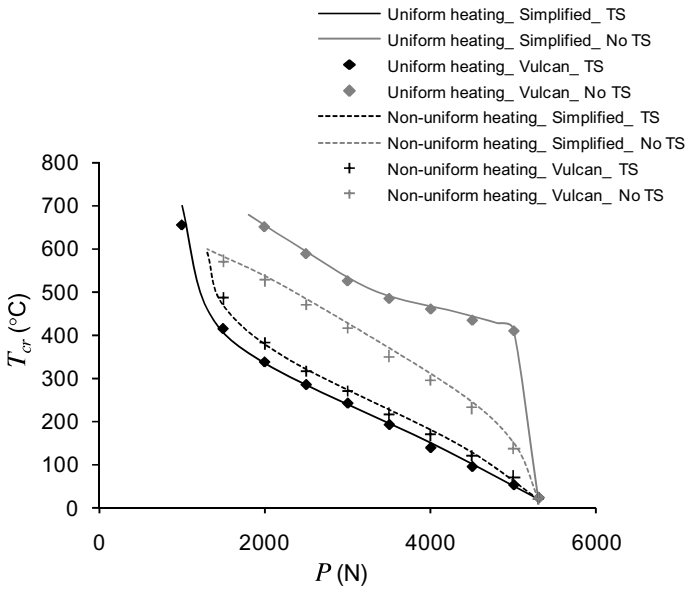

Figure 13 Buckling temperature of the concrete column against the applied load, predicted from *Vulcan* and the Shanley-like model.

Figure 14

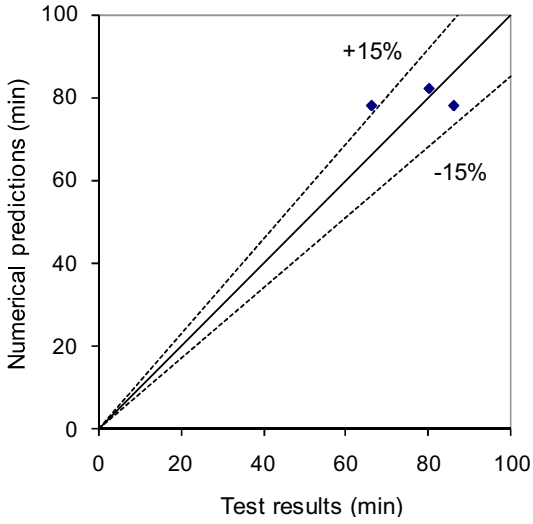

Figure 14 Comparison of the buckling resistance times given by tests and *Vulcan* analyses.

Figure 15

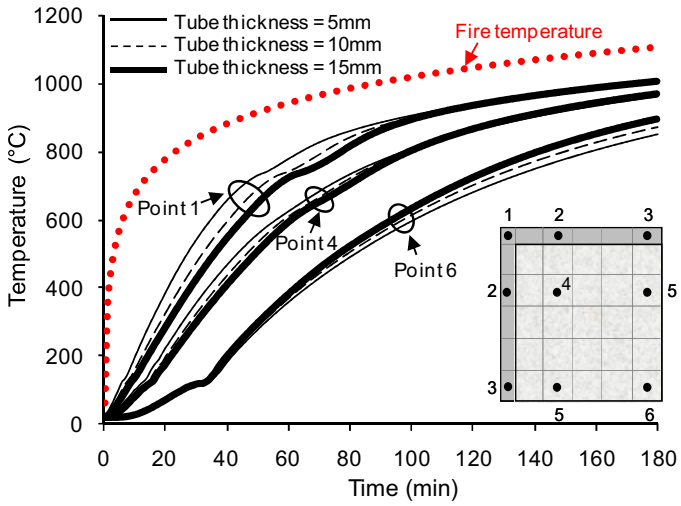

Figure 15 Temperature distributions across a quarter of the cross-section of CF1, CF2 and CF3.

Figure 16

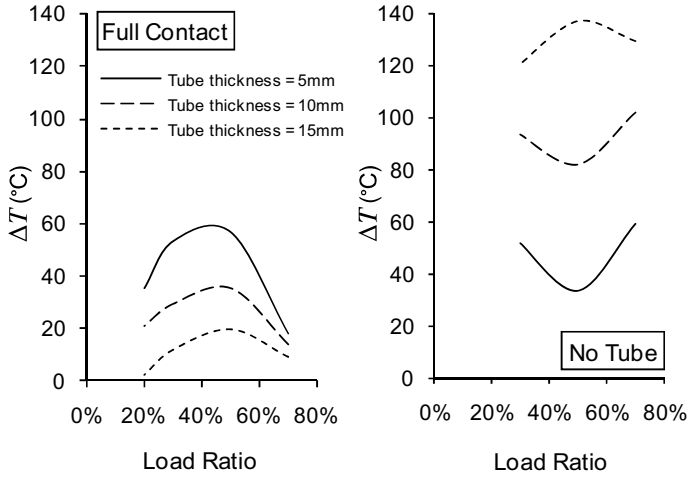

Figure 16 Reduction of the estimated buckling temperature due to the effect of TS, against the imposed load level, for columns of various tube thicknesses.

Figure 17

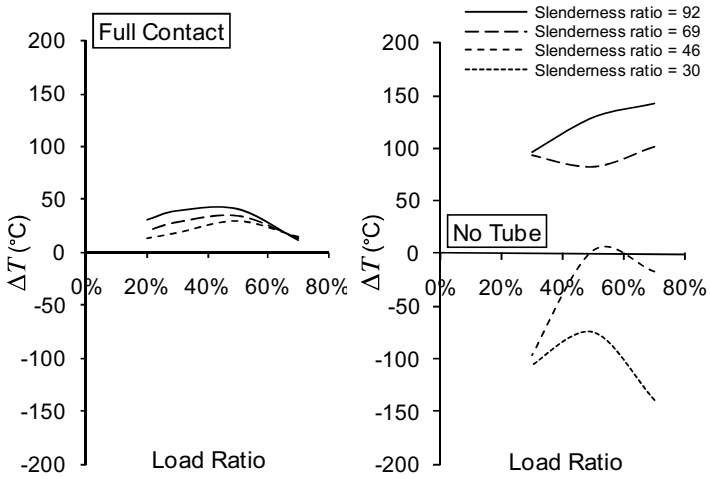

Figure 17 Reduction of the estimated buckling temperature due to the effect of TS, against the imposed load level, for columns of different slenderness.

Figure 18

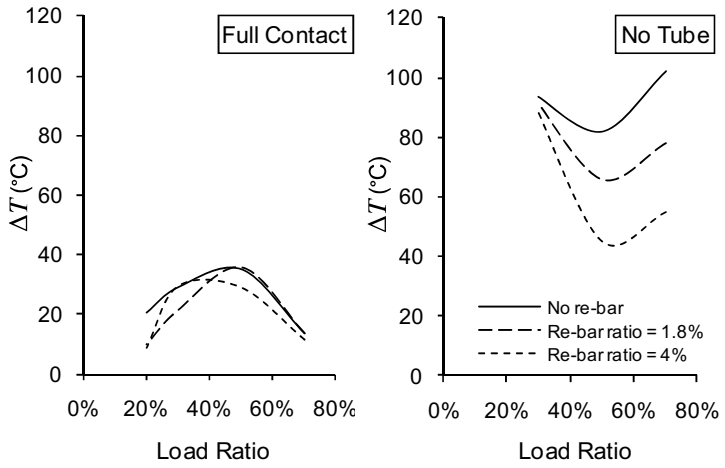

Figure 18 Reduction of the estimated buckling temperature due to the effect of TS, against the imposed load level, for columns of various reinforcement ratios.

Figure 19

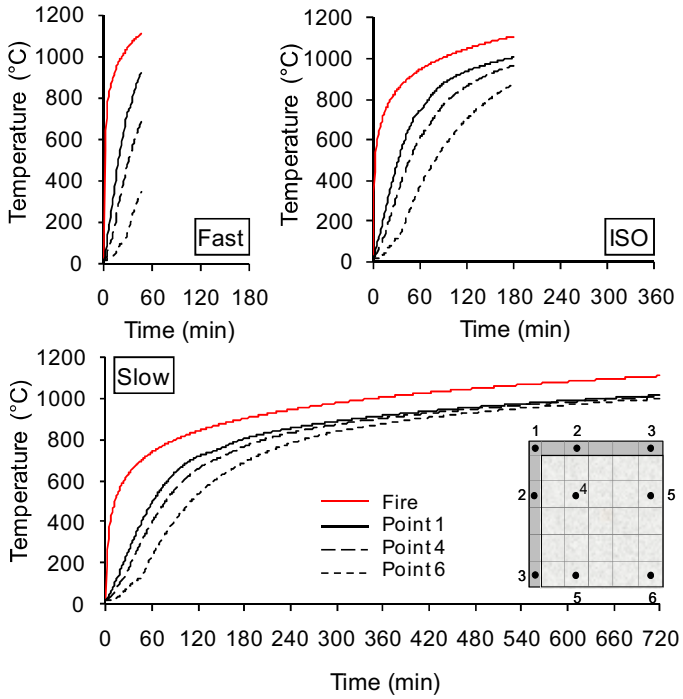

Figure 19 Temperature distributions across a quarter of the cross-section of CF2, heated at different rates.

Figure 20

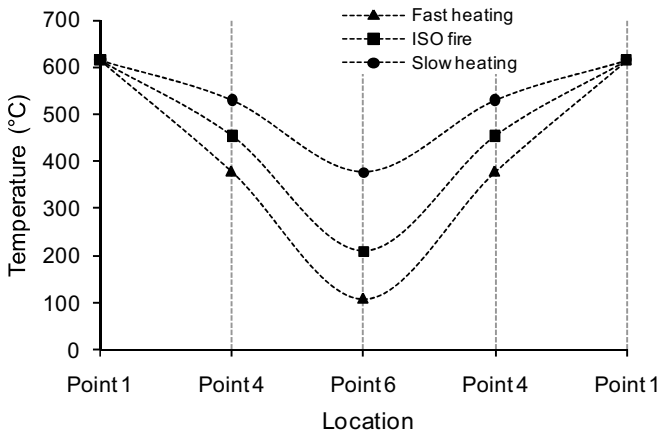

Figure 20 Temperature distributions across the column cross-section under different heating, at a surface temperature of 615°C.

Figure 21

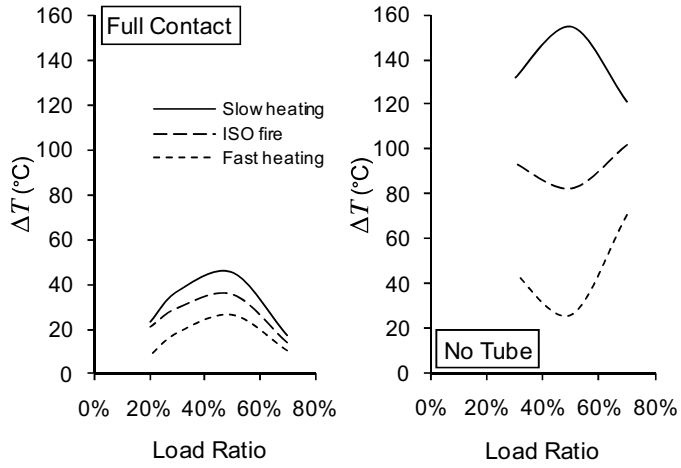

Figure 21 Reduction of the estimated buckling temperature due to the effect of TS, against the imposed load level, for columns under different heating.